Discovery of antibiotics and their targets in multidrug-resistant bacteria

Bakker, A.T.

Chapter 4

Chemical proteomics reveals antibiotic targets of oxadiazolones in MRSA

Introduction

The discovery of new drugs can be segmented in two ways: a target-based approach, or a phenotypic screening approach.[1] In the first method, the target-of-interest is determined from the onset, and this saves the effort of having to elucidate the drug's mode-of-action (MoA). Phenotypic screening, on the other hand, involves screening for the desired phenotypic effect, and afterwards pinpointing the exact MoA. Phenotypic screening is especially useful in the field of antibiotic drug discovery, where there are the added challenges of bacterial membrane permeability and efflux mechanisms to consider.[2–4] While phenotypic screening circumvents these barriers, elucidation of the MoA and corresponding targets is often challenging, especially in the case of multiple interacting partners.[5]

Recently, chemical proteomics has emerged as a powerful chemical biology technique to map target interaction landscapes of experimental drugs,[6–8] including compounds with antibacterial activity.[9,10] In particular, *in situ* competitive activity-based protein profiling (ABPP) makes it possible to profile protein targets of an inhibitor, by competing it against an activity-based probe (ABP). The ABP is a molecule that contains a specificity element to bind to proteins of interest, a warhead that can covalently trap reactive amino acids in the active sites of enzymes, and a reporter tag, that can be used for analysis of the trapped enzymes.

In Chapter 3, a structure-activity relationship (SAR) study was performed to optimize the antibacterial activity of oxadiazolone compound **1** against methicillin-resistant *Staphylococcus aureus* (Figure 4.1). Via improved scaffold **2**, this resulted in lead compound **3**, a compound with submicromolar antibacterial activity against MRSA, and similar activity against all tested clinical isolates. This is of high significance, as highly-resistant forms of *S. aureus* have been designated as dangerous pathogens, for which developing treatments with novel MoAs has high priority.[11,12]

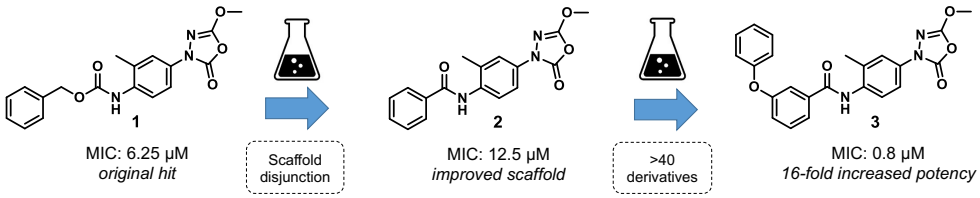

Figure 4.1 | Flow-chart from hit compound **1** to the simplified scaffold **2** to the optimized lead compound **3**.

The SAR study in Chapter 3 revealed that the oxadiazolone moiety is essential for antibacterial activity. Removal, or opening of the structure removes activity completely. Oxadiazolone-containing molecules have previously been shown to bind covalently to active-site serine and cysteine residues of lipases and proteins in *Mycobacteria* (Figure 4.2).[13–15] Therefore, the hypothesis is that the antibacterial activity of **3** is due to covalent modification of the active-site of bacterial enzymes in MRSA.

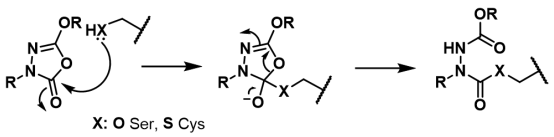

Figure 4.2 | Proposed reaction mechanism of 1,3,4-oxadiazole-2-one (oxadiazolone) derivatives towards reactive serine and cysteines.

In the context of this project, *in situ* competitive ABPP can be used to unravel the interacting protein targets of inhibitor **3** in MRSA. The idea is as follows (Figure 4.3): first an ABP is obtained that shares targets with the inhibitor of interest. The ABP provides the spectrum of proteins that inhibition can be measured of. The cells are first preincubated with an inhibitor, which results in certain target sites to be occupied, and thus, those are unavailable for probe labelling. Subsequent treatment with the ABP will result in the covalent labelling of unoccupied target enzyme sites. The inhibited sites can be uncovered by comparing the signal

of probed sample without inhibitor preincubation to that with inhibitor preincubation. This is done by first lysing the cells after probe labelling, and then installing a reporter tag by performing copper-catalyzed azide–alkyne cycloaddition (CuAAC) ("click") chemistry. This can either be a fluorophore tag for sodium dodecyl sulfate polyacrylamide gel electrophoresis (SDS-PAGE) gel visualization, or a biotin enrichment tag for biotin-streptavidin pulldown, followed by tryptic digestion, and MS-analysis of the resulting peptides to determine the inhibited proteins.

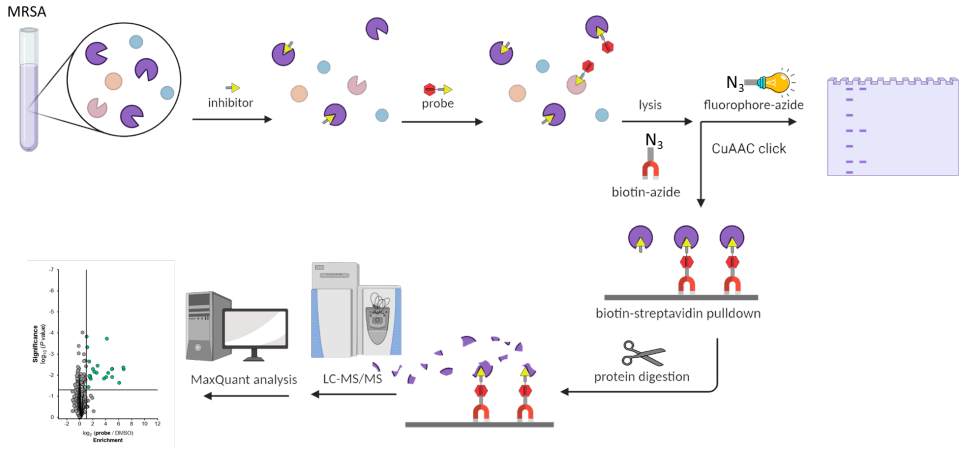

Figure 4.3 | *In situ* competitive ABPP workflow. Schematic overview of the *in situ* competitive activity-based protein profiling (ABPP) workflow on MRSA using either SDS-PAGE or mass-spectrometry read-out.

In this chapter, the targets of the oxadiazolone compounds in MRSA are elucidated by competitive chemical proteomics assays. The chemical probe was carefully chosen based on bioactivity and shared targets with the lead compound. Additional studies on transposon mutants and generated oxadiazolone-resistant mutants revealed several cysteine and serine hydrolases as most relevant targets. These data showcase oxadiazolones as a novel highly potent antistaphylococcal chemotype with a polypharmacological mode-of-action.

Results

Selecting a suitable probe. Due to the reported reactivity of oxadiazolone compounds with serine hydrolases, it was surmised that a serine hydrolase-binding ABP might be suitable to uncover relevant targets. Fluorophosphonate-based probes are the original class of ABPs that can covalently bind a wide variety of serine hydrolases.[16] To that end, FP-alkyne (Figure 4.4),[17] an alkynylated fluorophosphonate probe, was tested for *in situ* serine hydrolase labelling on MRSA cells. In a gel-based experiment (Figure S4.1), FP-alkyne labelled a considerable number of proteins at low dosages. However, it was found that, even up to a 50 μM concentration, FP-alkyne did not show any antibacterial activity. It was reasoned that the target profile of a non-bioactive probe would not contain the full target spectrum of which inhibition results in antibacterial activity. Therefore, it was decided that FP-alkyne was not a suitable probe for unraveling the targets related to the antibacterial activity of the oxadiazolones.

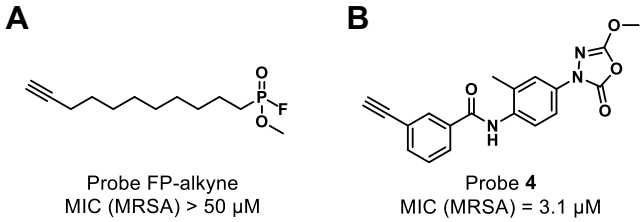

Figure 4.4 | Probes tested for profiling oxadiazolone targets. A) Activity-based probe FP-alkyne, used to profile serine hydrolases. **B)** Activity-based probe **4**, based on the scaffold of lead compound **3**.

The oxadiazolone moiety covalently reacts with catalytically active amino acids in enzymes, which implicated that a strategically positioned alkyne ligation handle on the scaffold of **3** could be used to make an oxadiazolone-based ABP. To this end, the most potent alkyne-bearing derivative synthesized in Chapter 3, compound **4** (MIC = 3.1 μM), was chosen for further investigation (Figure 4.4). To check if the probe had a covalent binding mode, MRSA was incubated with probe **4**, and subsequently functionalized with a fluorescent Alexa647-azide. This resulted in clear labelling by **4** of several proteins, of which most targets could be dose-dependently outcompeted by lead compound **3** (Figure 4.5).

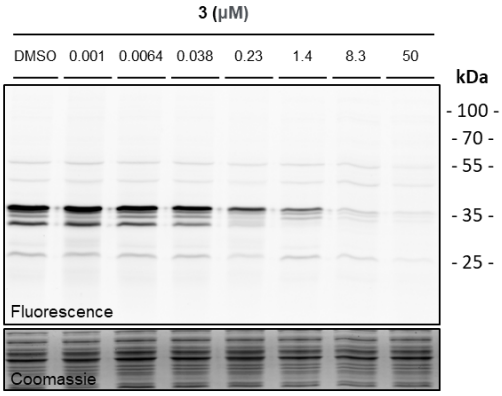

Figure 4.5 | Gel-based competitive ABPP of a concentration range of compound **3** (1 nM to 50 μM) versus probe **4** (1 μM).

Identification of oxadiazolone targets. Having established that probe **4** is bioactive and can covalently label proteins, of which most are outcompeted by compound **3**, the next step was to identify the probe-labelled proteins. This was done by coupling the probe **4**-labelled proteins to a biotin reporter group, which allows affinity enrichment and identification of probe-labelled proteins by mass spectrometry (MS)-based proteomics.[19] 21 proteins were found to be significantly enriched ($p < 0.05$, > 2-fold enrichment) by probe treatment (Figure S4.2, Table S4.1). Pretreatment with **3** significantly inhibited ($p < 0.05$, > 2-fold inhibition) the labelling of 10 proteins by probe **4** (Figure 4.6, Table 4.1), suggesting that these proteins are the most prevalent interaction partners of oxadiazolone **3**.

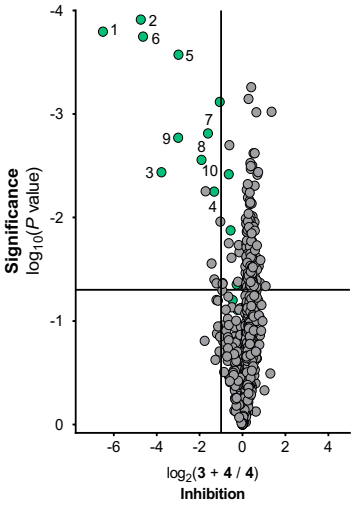

Figure 4.6 | Mass spectrometry data inhibition plot comparing labelled proteome of samples preincubated with inhibitor **3** (10 μM) followed by labelling with probe **4** (3 μM), to solely probe **4** labelled (3 μM) samples. Significantly inhibited probe targets (>2-fold inhibition, $p < 0.05$) are numbered 1 to 10, and detailed in Table 4.1.

Table 4.1 | List of probe targets significantly outcompeted by compound **3** (Figure 4.6).

#	Uniprot ID	Protein	Description	Sequence length (aa)	Gene	Essential	References
1	Q2FDS6	FphE	Uncharacterized hydrolase	276	SAUSA300_2518	No	20, 21
2	Q2FI93	FabH	3-oxoacyl-[acyl-carrier-protein] synthase 3	313	*fabH*	Yes	22–25
3	A0A0H2XJL0	FphH	Carboxylesterase	246	*est*	No	20
4	A0A0H2XHZ1	HZ1	Putative lysophospholipase	271	SAUSA300_0070	No	
5	A0A0H2XHD0	FphC	Hydrolase. alpha/beta hydrolase fold family	304	SAUSA300_1194	No	20
6	A0A0H2XHH9	HH9	Putative lipase/esterase	347	SAUSA300_0641	No	
7	A0A0H2XJG5	FphB	Uncharacterized protein	322	SAUSA300_2473	No	20
8	A0A0H2XFI2	FI2	Uncharacterized protein	275	SAUSA300_0321	No	
9	A0A0H2XIB7	IB7	Acetyl-CoA c-acetyltransferase	379	*vraB*	No	26
10	A0A0H2XG10	AdhE	Aldehyde-alcohol dehydrogenase	869	*adhE*	No	27–29

Four of the proteins (FphB, C, E and H) were recently discovered and annotated in MRSA as fluorophosphonate binding hydrolases (Fph's).[20] FphB was found to be a fatty acid metabolizing virulence factor, while FphE activity has been used to phenotypically characterize MRSA through imaging.[21] Target proteins HZ1 and HH9 are reported to have hydrolase activity, but their biological function has not been extensively studied. IB7 is a putative acetyl-CoA c-acetyltransferase with thiolase activity,[26] while FI2 is an uncharacterized protein. FabH also known as 3-oxoacyl-[acyl-carrier-protein] synthase 3 is an essential enzyme that initiates bacterial fatty acid synthesis[23], and has recently been explored as a drug target.[22,24,25] AdhE is an aldehyde alcohol dehydrogenase, essential in facultative anaerobic organisms in anaerobic conditions.[27,28] Both FabH and AdhE are known to metabolize substrates using an active site cysteine.

To confirm the identity of the probe targets with gel-based ABPP, nine transposon mutant strains were obtained that effectively lack the genes encoding for our probe targets. By virtue of the absence of probe labelling the probe bands could then be identified. The labelling of AdhE, FphB, FphE, FphH, FI2 and HZ1, but not FphC and HH9, could be attributed to specific fluorescent bands on SDS-PAGE (Figure 4.7). The lower resolution of gel-based ABPP (overlapping bands) or insufficient sensitivity compared to MS-based ABPP may explain why FphC and HH9 were not identified on gel. Since FabH is essential for MRSA viability, no transposon mutant is available for this protein. Instead, we confirmed the identity of FabH on gel by competitive ABPP using the selective FabH inhibitor Oxa2 (Figure S4.3).

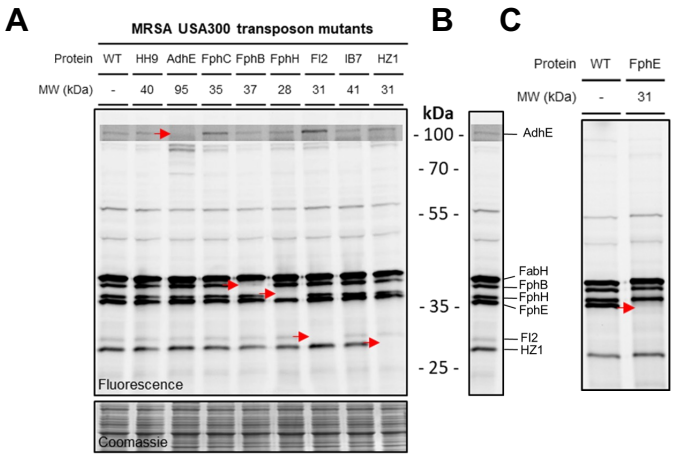

Figure 4.7 | Identification of targets ABP 4 on gel. A) 4 labelling of MRSA USA300 transposon mutant strains, each with a transposon sequence inserted in genes of all identified **4** targets, except FabH and FphE. **B)** Legend of **4** probe labelling bands In MRSA USA300 WT annotated with corresponding proteins. **C) 4** labelling of MRSA USA300 FphE transposon mutant compared to WT.

Zooming in on the targets relevant for antibacterial activity. To assess which target proteins were responsible for the antibiotic effect, it was hypothesized that the protein inhibition profile of potent oxadiazolones (MIC ≤ 12.5 μM) would be different compared to the interaction profile of their close analogues with no activity (MIC > 50 μM). In a competitive chemical proteomics set-up, therefore, the interaction profile of three inactive derivatives (**5**-**7**) was compared with that of three active compounds (**1**-**3)** (Figure 4.8, 4.9 and S4.4).

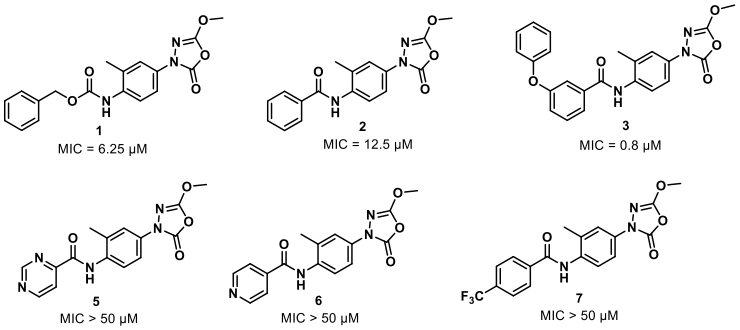

Figure 4.8 | Structures of selected active compounds **1**-**3** and inactive compounds **5**-**7**, along with their MIC values in MRSA USA300.

Strong FphB inhibition was seen in the samples pretreated with **1**, but not by the other compounds. F12, IB7, HH9 and HZ1 were not significantly inhibited by the bioactive oxadiazolone **3**, but did show engagement by the inactive compounds **5, 6** or **7**. FphE and FphH were strongly inhibited by all compounds. These observations in combination with the viability of the transposon mutants suggest that FphB, IB7, HH9, F12, FphE, FphH and HZ1 are not essential for the antimicrobial activity of **3** on their own. However, it cannot be excluded that inhibition of these enzymes is partially responsible for the antibacterial effects

observed. FabH was significantly engaged, but not fully, by all compounds. Since the transposon mutant of FabH is not viable, this implies that partial inhibition of FabH activity could contribute to the bioactivity of the oxadiazolones, however, it is not sufficient to stop MRSA by itself. Finally, significant inhibition of FphC and AdhE labelling was only found in the bioactive compounds, but not by the inactive compounds **5-7** (Figure 4.9B).

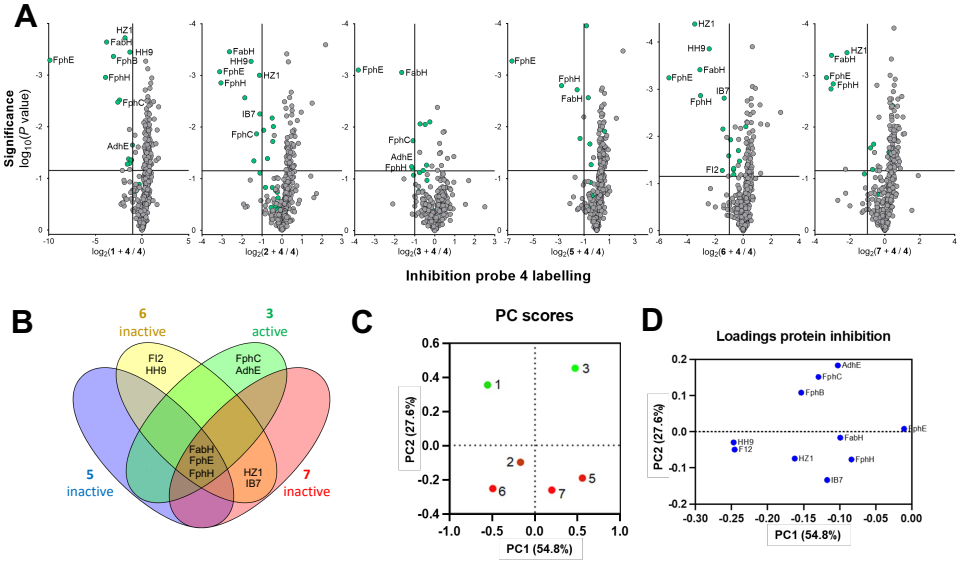

Figure 4.9 | Activity-based proteomics predicts protein inhibition relevant to antibacterial effect. A) Individual inhibition plots of a selection of active and inactive compounds. **3** was dosed at 1 µM, while the other inhibitors were dosed at 10 µM. **B)** Venn diagram showing overlap of >50% inhibited proteins between active compound **3** and three inactive compounds **5**-**7**. **C)** PCA analysis of the inhibition profiles of the six compounds. **D)** Contribution of individual protein inhibition levels to PC1 and PC2.

Principal component analysis (PCA) of the chemical proteomics data gave quantitative confirmation that inhibition of AdhE and FphC activity was correlated to a large extent with the antibacterially active compounds (Figure 4.9D, Table S4.2). The chemical proteomic data thus warrant further investigation of AdhE and FphC as interesting targets beside FabH.

To follow up on this, the question was whether antibiotic activity of the inactive compounds **5-7** could be induced in the FphC and AdhE transposon mutants. Gratifyingly, it was observed that both **6** and **7** showed increased antimicrobial activity in both transposon mutants (Table 4.2), but not in a FphB transposon mutant, which was taken along as a negative control. Of interest, compounds **6** and **7** did not become as active as **3**. Compound **5**, which has no activity on AdhE and very weak activity on FphC (< 20%), remained inactive in all individual transposon mutants. Although it cannot be excluded that other proteins also play a role, these data can be interpreted to mean that combined engagement of FphC and AdhE is required for antimicrobial activity of the oxadiazolones.

Table 4.2 | MIC values MRSA USA300 transposon mutants of target proteins

MRSA USA300 strain	MIC (μM)		
	Inactive **5**	Inactive **6**	Inactive **7**
WT	>50	>50	>50
AdhE transposon mutant	>50	25	12.5
FphC transposon mutant	>50	50	25
FphB transposon mutant	>50	>50	>50

Besides FphC and AdhE, the other transposon mutants were also tested for antimicrobial susceptibility (Table S4.3) to oxadiazolones. The FphE transposon mutant showed significantly higher sensitivity to compounds **2** and **7**. This was an interesting observation as these compounds already showed a high degree of FphE inhibition (Figure S4.4, ±80% inhibition), although the other compounds showed stronger inhibition.

Target activity-changes in oxadiazolone-resistant MRSA mutants. A common way of identifying targets of antibiotics, is by inducing resistance in otherwise susceptible bacteria and then screening its genome for mutations that might cause the resistance. A quick way to obtain resistant bacteria is by growing a culture on agar containing an antibiotic concentration that normally prevents growth. Viable colonies are highly likely to harbor resistance to the antibiotic. To achieve this, agar containing compound **3** (5x MIC) was inoculated with MRSA, and the following day several colonies were isolated and tested for susceptibility to **3**. The isolated colonies only had low resistance to compound **3** (2-4x MIC), and the resistance was found to be unstable as it reverted within several days.

To generate strains with higher levels of resistance, MRSA was serially passaged daily in the presence of sub-MIC concentrations of compound **3**. This yielded highly resistant mutants after 4 weeks (Figure 4.10). In comparison, resistance development for the control compound daptomycin, a clinically-used lipopeptide antibiotic, was found to be slower and did not exceed 8x MIC. This is commonly observed in cell membrane targeting antibiotics.[30,31]

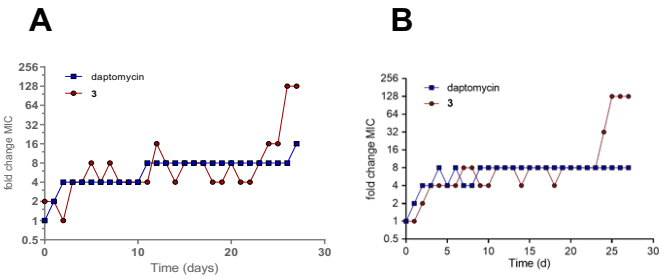

Figure 4.10 | Resistance development of MRSA USA300 against **3** and daptomycin during daily serial passaging with 0.25x MIC concentrations in two biological replicates. At the final point colonies were isolated and labelled **A)** MRSA USA300 **3**-resistant A, and **B)** MRSA USA300 **3**-resistant B.

Of note, after four days the resistance towards **3** stabilized for several weeks before progressing to significantly higher values. This may indicate that multiple mutations are required to fully induce resistance, supporting a polypharmacological MoA. **3**-resistant mutant strains did not show cross-resistance with commonly administered antibiotics (Table S4.4). Interestingly, Oxa2 was found to be 32x less potent in both **3**-resistant strains. This highly suggests mutations in FabH, the main target of Oxa2, and the only essential target of compound **3**.

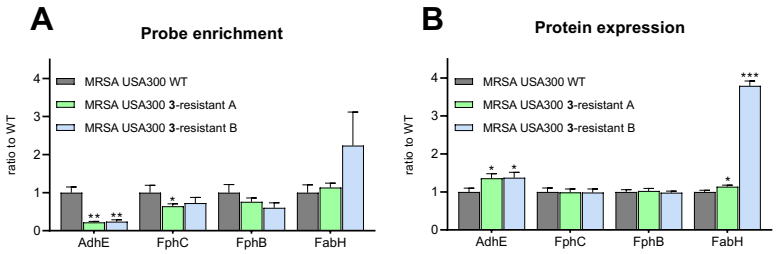

Figure 4.11 | Protein profiles 3-resistant mutants vs WT. A) Relative protein levels enriched by **4** in **3**-resistant strains compared to WT. **B)** Relative general protein levels in **3**-resistant strains compared to WT.

With the resistant strains in hand, it was investigated whether FphC and AdhE activity was changed in the **3**-resistant MRSA strains compared to WT MRSA. Using chemical (Figure 4.11A and S4.5A) and global proteomics (Figure 4.11B and S4.5B) it was observed that AdhE activity was significantly decreased to 20% in both strains, while the general protein abundance was significantly upregulated. FphC-activity was also reduced, but to a lower extent. Interestingly, FabH protein levels were significantly increased in the resistant strains. Extended data (Figure S4.5) shows FphE expression to be significantly upregulated in both resistant strains, while probe labelling is reduced.

Discussion

To summarize, a phenotypic screen of a focused library led to the identification of oxadiazolones as a new chemotype with antibiotic activity against pathogenic, multidrug resistant *S. aureus* strains and clinical isolates. A medicinal chemistry program combined with chemical proteomics led to the identification of compound **3** as the most potent antibiotic capable of interacting with multiple bacterial cysteine and serine hydrolases in a covalent manner. Three complementary lines of investigation point to FabH, FphC and AdhE as playing central roles in the antimicrobial activity of **3** and structurally similar oxadiazolones: i) comparative chemical proteomics, ii) gain of function in transposon mutants, and iii) resistance-induced proteomic changes. FabH has previously been identified as a drug target, whereas the function of AdhE and FphC has been less well explored. Recent studies implicate AdhE as a virulence factor in *E. coli*,[29] while FphC is a predicted membrane-bound serine hydrolase of unknown function. Of note, it cannot be ruled out that other factors, not detected by the chemical proteomics approach, may also contribute to the antibacterial effect of **3**, such as non-covalent interactions with proteins or other classes of biomolecules.

Interestingly, the resistance developed to **3** was transient in a single-step resistance assay, as it quick diminished after several days of culturing without antibiotic. Highly resistant bacteria were obtained by daily serial passage with compound **3**. However, it remains to be investigated if this resistance is 1) stable, and 2) a result of mutations in target proteins.

To conclude, these findings further highlight the value of synthetic compound libraries as an excellent source for antibiotic drug discovery complementary to natural products. By applying comparative and competitive chemical proteomics, using a new tailor-made activity-based probe with a strategically positioned ligation tag, I successfully elucidated the most notable protein targets of oxadiazolones in MRSA, along with the implied targets responsible for the antibacterial effect.

Notably, a target-based approach alone would have not been able to uncover the mode-of-action of the oxadiazolones, thereby showcasing the power of chemical proteomics as a valuable chemical biology technique for antibiotic drug discovery. Future experiments are directed towards understanding the biological role of these targets and further optimization of the compounds as viable drug candidates.

Acknowledgments

The following people are kindly acknowledged for their contribution to this chapter. Verena Straub for optimization of the ABPP protocol in MRSA, and Ioli Kotsogianni for creating the **3**-resistant mutant strains, and assisting with the antimicrobial assays. The lab of prof. dr. Matthew Bogyo is thanked for supplying the FphE transposon mutant, and the Network on Antimicrobial Resistance in *Staphylococcus aureus* (NARSA) is thanked for supplying the remaining transposon mutants (NTML). Bobby Florea is thanked for measuring the proteomics samples.

Methods

Reagents & materials. Buffers and salts were of ACS reagent grade or higher and were purchased commercially, from Carl Roth GmbH (Karlsruhe, Germany) and Sigma-Aldrich (Darmstadt, Germany), biological materials and growth media were purchased from Sigma-Aldrich, Scharlab S.L. (Barcelona, Spain) and Fisher Scientific (Landsmeer, Netherlands). Antibiotics (TRC, Combi-Blocks, Sigma-Aldrich) were dissolved in ultrapure H_2O or DMSO, stock solutions were stored at -20°C. Test compounds were used from 10 mM DMSO stock solutions made from freeze-dried powder and stored at -20°C.

Bacterial strains. The following *S. aureus* strains were provided by the Network on Antimicrobial Resistance in *S. aureus* (NARSA) for distribution by BEI Resources, NIAID, NIH: JE2 Transposon Mutants: NE114 (SAUSA300_0151, NR-46657), NE204 (SAUSA300_1194, NR-46747), NE104 (SAUSA300_0641, NR-46647), NE1534 (SAUSA300_0070, NR-48076), NE1227 (SAUSA300_0560, NR-47770), NE532 (SAUSA300_2473, NR-47075) NE1122 (SAUSA300_0763, NR-47665), NE1187 (SAUSA300_0321, NR-47730), NE31 (SAUSA300_2093, NR-46574). *S. aureus* USA300 (ATCC BAA1717), *S. aureus* Rosenbach (ATCC 29213) belong to the American Type Culture Collection (ATCC).

Minimum inhibitory concentration (MIC). From glycerol stocks, bacterial strains were cultured on blood agar plates by overnight incubation at 37°C. A single colony was transferred to TSB. In case of VRSA strains, 6 μg/mL vancomycin was supplemented to the media. The cultures were grown to exponential phase (OD_{600}: 0.5) at 37°C. The bacterial suspensions were diluted 100-fold in CAMHB and 50 μL was added to a 2-fold serial dilution series of test compounds (50 μL per well) in polypropylene 96-well microtiter plates to reach a volume of 100 μL. The plates were sealed with breathable membranes and incubated overnight at 37°C with constant shaking (600 rpm). For *Enterococci species* direct colony suspension was used by immediately suspending multiple colonies from fresh blood agar plates in CAMHB to an OD_{600} of 0.5 and subsequent 100-fold dilution. The MIC was determined as the lowest concentration at which no visible bacterial growth was observed, as compared to the inoculum controls, from the median of a minimum of triplicates.

Resistance induction assay. From glycerol stocks, bacterial strains were cultured on blood agar plates by overnight incubation at 37°C. A single colony was grown to exponential phase (OD600 = 0.5) in TSB and diluted 100-fold in fresh media. In polypropylene 96-well microtiter plates, antibiotics were added in biological triplicates and serial diluted 2-fold by transfer and mixing from one well to the next to achieve a final volume of 50 μL per well. An equal volume of bacterial suspension was added to the wells and plates were incubated at 37°C for 18 h. Bacterial cultures corresponding to 0.25× MIC were diluted 100-fold in fresh media and added (50 μL per well) to a newly prepared antibiotic dilution series (50 μL per well) followed by incubation at 37°C for 18 h. This procedure was repeated for 30 days and the MIC was recorded daily. The experiment was performed in biological triplicates and for each replicate the MIC was determined from the median of a minimum of triplicates.

Sample preparation ABPP. Several bacterial colonies were suspended in LB medium in sterile Erlenmeyer flasks and grown in aerobic conditions at 37°C shaking at 270 rpm. At an OD600 of at least 0.70, the cells were divided in 50 mL fractions and harvested by centrifugation (5000 rcf, 10 min, 4°C), and were then washed with PBS once. For each fraction, the pellet was resuspended in 1000 μl PBS, then the samples were pooled and divided into 396 μl samples in 1.5 mL Eppendorf tubes. To each sample 1.5 μl DMSO or inhibitor (200× concentrated) was added and the samples were incubated (600 rpm, 37°C, 1 h). 1.5 μl probe (200× concentrated, final concentration 3 μM) or DMSO was then added and the samples were incubated (37°C, 600 rpm, 30 min).

Cells were pelleted by centrifugation (5000 rcf, 10 min, 4°C) and washed with PBS once. Pellets were then resuspended in 300 μl PBS/0.2% SDS (+ Roche cOmplete protease inhibitor cocktail) and lysed by bead beating (3× 50 s at 6 m/s).

Gel-based ABPP and in-gel fluorescence analysis. 18 µl of lysate was clicked with Alexa647-azide (Invitrogen, A10277) by adding 2 µl click mix (10×, 10 mM $CuSO_4$, 56.56 mM sodium ascorbate, 2 mM THPTA, 40 µM Alexa647-azide in Milli-Q) and incubating at rt for 1 h. Note: prepare the click mix separately and in the listed order. The reaction was quenched by addition of 5 µl Laemmli buffer (4×, 240 mM Tris-HCl pH 6.8, 8% w/v SDS, 40% glycerol, 5% v/v β-mercapto-ethanol, 0.04% v/v bromophenol blue), followed by heating (95°C, 5 min). The samples were resolved by SDS-PAGE (12.5% acrylamide gel, 15-wells, 10 µL per well) at 180V for 80 min, after which the gels were imaged at Cy3 and Cy5 channels on a ChemiDoc Imaging System (Bio-Rad). Gels are controlled for equal protein loading with Coomassie Brilliant Blue staining. Images were processed using ImageLab software (Bio-Rad).

Preparation for LC-MS based ABPP. Sample preparation was performed according to literature[18] with slight changes. 275 µl of lysate was clicked with biotin-azide (Cayman Chemical, 13040) by adding 25 µl click mix (10×, 10 mM $CuSO_4$, 56.56 mM sodium ascorbate, 2 mM THPTA, 0.4 mM biotin-azide in Milli-Q) and incubating at rt for 1 h. Note: prepare the click mix separately and in the exact order listed.

To each sample 170 µl Milli-Q was added to create a final volume of 500 µl. In the following steps samples were vortexed after each addition. First, 666 µl MeOH was added, then 166 µl chloroform, and finally 150 µl of Milli-Q. Samples were centrifuged (10 min, 1500 g), and solvents were carefully removed respecting the integrity of the formed protein pellet. MeOH (600 µL) was added and the pellet was resuspended using a probe sonicator (30% amplitude, 10 s). The samples were centrifuged (5 min, 18,400 g), and the solvent was removed, again carefully. The residual protein pellet was then dissolved in urea buffer (250 µL, 6 M urea, 250 mM NH_4HCO_3) by means of pipetting.

To each sample DTT (2.5 µL 1 M stock, final concentration 10 mM) was added, followed by incubation at 65°C for 15 minutes while shaking (600 rpm). Samples were cooled to RT and iodoacetamide (20 µL 0.5 M stock, final concentration 40 mM) was added, afterwards keeping the samples dark for 15 minutes. SDS (70 µL 10% stock, final concentration 2%) was added, and the samples were incubated for 5 minutes at 65°C while shaking (600 rpm). 1.2 mL of avidin agarose beads (ThermoFisher, 20219) were divided over four 15 mL tubes, and washed with PBS (by adding PBS (10 mL per tube), centrifugation (2 min, 2500 g) and removal of the PBS. Bead solution was made by adding PBS (6 mL) to each of the four tubes. Each of the SDS treated samples were transferred to a 15 mL tube, along with bead solution (1 mL) and PBS (2 mL). The sample containing tubes were rotated for 3 h using an overhead shaker. After shaking, the samples were centrifuged (2 min, 2500 g) and the supernatant was removed. Samples were then resuspended in 0.5% SDS in PBS (6 mL), followed by similar centrifugation (2 min, 2500 g) and removal of supernatant. This process was then repeated thrice with PBS (6 mL), leaving a washed bead pellet. On-bead digestion buffer (250 µL, 100 mM Tris pH 8.0, 100 mM NaCl, 1 mM $CaCl_2$, 2% ACN) was added to the each of the bead residues, and the beads were transferred to low binding tubes (1.5 mL, Sarstedt). Each sample was treated with trypsin solution (1 µL, 0.5 µg/µL Sequencing Grade Modified Trypsin, Porcine (Promega) in 0.1 mM HCl), and the samples were incubated at 37°C overnight while shaking (950 rpm).

To each sample formic acid (12.5 µL) was added, followed by filtering off the beads over biospin columns (Bio-Rad, 7326204) on top of 2 mL Eppendorf tubes using centrifugation (2 min, 300 g). Note: the 2 mL Eppendorf tubes now contain sample solution. StageTips were used for subsequent desalting of the samples. StageTips are punched through holes in Eppendorf tubes, which collect flow-through and each individual step is followed by centrifugation (2 min, 300 g). The StageTips were treated by first conditioning with MeOH (50 µL), washing with solution B (50 µL, 80% v/v MECN, 0.5% v/v formic acid in Milli-Q), and solution A (0.5% v/v formic acid in Milli-Q). The sample solution is then loaded through StageTips, followed by a wash with solution A (50 µL). The StageTips are then transferred to low binding tubes, and the tips are flushed with solution B (100 µL). The collected flow-through is concentrated *in vacuo* using a SpeedVac (Eppendorf Concentrator 5301) at 45°C for 3 h. The samples are stored at at -20°C until LC-MS measurement.

Preparation for full proteome analysis. Bacterial cell lysate was obtained following the 'Sample preparation ABPP' protocol, with minor changes: 1) LB medium was supplemented with either DMSO or 0.78 µM inhibitor during initial bacterial culture; 2) after harvesting, the cells were directly lysed.

Following cell lysis, protein precipitation was performed as described, and protein concentration was determined using a BCA assay. Per sample, an amount of protein solution was taken corresponding to 250 µg of protein, and this was diluted with urea buffer to 1 mg/mL protein (250 µL) total. This was followed by adding DTT (5 mM final concentration), and shaking (15 min, 900 rcf, 65°C). After this IAA (40 mM final concentration) was added and the samples were incubated in the dark for 30 min.

For digestion, 100 µL of sample was transferred to a LoBind Eppendorf tube and diluted with 500 µL OB-DIG buffer, and 1 µg trypsin (2 µL, 0.5 µg/µL solution in 1 mM HCl, Promega) was added. The samples were incubated o/n (950 rcf, 37°C). Formic acid (50 µL) was added to quench the reaction and the samples were desalted as reported in 'Preparation for LC-MS based ABPP'.

LC-MS measurement and analysis. Desalted peptide samples were reconstituted in LC-MS solution (3% v/v MECN, 0.1% v/v formic acid in Milli-Q, 50 µL for ABPP samples, 100 µL for full proteome samples) containing 10 fmol/µL yeast enolase digest (cat. 186002325, Waters). Injection amount was titrated using a pooled quality control sample to prevent overloading the nanoLC system and the automatic gain control (AGC) of the QExactive mass spectrometer.

The desalted peptides were separated on an UltiMate 3000 RSLCnano system set in a trap-elute configuration with a nanoEase M/Z Symmetry C18 100 Å, 5 µm, 180 µm × 20 mm (Waters) trap column for peptide loading/retention and nanoEase M/Z HSS C18 T3 100 Å, 1.8 µm, 75 µm × 250 mm (Waters) analytical column for peptide separation. The column was kept at 40°C in a column oven. Samples were injected on the trap column at a flow rate of 15 µL/min for 2 min with 99% mobile phase A (0.1% FA in ULC-MS grade water (Biosolve)), 1% mobile phase B (0.1% FA in ULC-MS grade MECN (Biosolve)) eluent.

For ABPP experiments, an 85 min LC method, using mobile phase A and mobile phase B controlled by a flow sensor at 0.3 µL/min with average pressure of 400-500 bar (5500-7000 psi), was programmed as gradient with linear increment to 1% B from 0 to 2 min, 5% B at 5 min, 22% B at 55 min, 40% B at 64 min, 90% B at 65 to 74 min and 1% B at 75 to 85 min. The eluent was introduced by electro-spray ionization (ESI) via the nanoESI source (Thermo) using stainless steel Nano-bore emitters (40 mm, OD 1/32", ES542, Thermo Scientific).

For full proteome experiments, a 123 min LC method, using mobile phase A and mobile phase B controlled by a flow sensor at 0.3 µL/min with average pressure of 400-500 bar (5500-7000 psi), was programmed as gradient with linear increment to 1% to 5% B from 0 to 2 min, 5% to 13% B from 2 to 63 min, 13% to 22% B from 63 to 85 min, 22% to 40% B from 85 to 104 min, 90% at 105 min and kept at 90% to 113 min. The eluent was introduced by electro-spray ionization (ESI) via the nanoESI source (Thermo) using stainless steel Nano-bore emitters (40 mm, OD 1/32", ES542, Thermo Scientific).

The QExactive HF was operated in positive mode with data dependent acquisition without the use of lock mass, default charge of 2+ and external calibration with LTQ Velos ESI positive ion calibration solution (88323, Pierce, Thermo) every 5 days to less than 2 ppm. The tune file for the survey scan was set to scan range of 350 – 1400 m/z, 120,000 resolution (m/z 200), 1 microscan, automatic gain control (AGC) of 3e6, max injection time of 100 ms, no sheath, aux or sweep gas, spray voltage ranging from 1.7 to 3.0 kV, capillary temp of 250°C and an S-lens value of 80. For the 10 data dependent MS/MS events the loop count was set to 10 and the general settings were resolution to 15,000, AGC target 1e5, max IT time 50 ms, isolation window of 1.6 m/z, fixed first mass of 120 m/z and normalized collision energy (NCE) of 28 eV. For individual peaks the data dependent settings were 1.00e3 for the minimum AGC target yielding an intensity threshold of 2.0e4 that needs to be reached prior of triggering an MS/MS event. No apex trigger was used, unassigned, +1 and charges >+8 were excluded with peptide match mode preferred, isotope exclusion on and dynamic exclusion of 10 sec.

In between experiments, routine wash and control runs were done by injecting 5 µl LC-MS solution containing 5 µL of 10 fmol/µL bovine serum albumin (BSA) or enolase digest and 1 µL of 10 fmol/µL angiotensin III (Fluka, Thermo)/oxytocin (Merck) to check the performance of the platform on each component (nano-LC, the mass spectrometer (mass calibration/quality of ion selection and fragmentation) and the search engine).

MS data analysis and processing. Raw files were analyzed using MaxQuant software (version 1.6.17.0) with the Andromeda search engine. The following settings were applied: fixed modification: carbamidomethylation (cysteine); variable modification: oxidation (methionine), acetylation (N-terminus); proteolytic enzyme: trypsin/P; missed cleavages: 2; main search tolerance: 4.5 ppm; MS/MS tolerance: 0.5 Da; false discovery rates: 0.01. The options "LFQ" and "match between runs" (0.7 min match and 20 min alignment time windows) were enabled; "second peptides" was disabled. Searches were performed against the UniProt database for the *S. aureus* USA300 proteome (Uniprot ID: UP000001939, downloaded 03-05-2019). Data was extracted from the "peptides.txt" and "proteingroups.txt" files.

For competitive proteomics, values were corrected by background signal subtraction in Excel, using no probe DMSO control sample for background measurement (negative values rounded to 0). Statistical analysis of the data was performed using Perseus (version 1.6.15.0). Putative contaminants, reverse peptides and peptides only identified by site were deleted. LFQ intensities were log2-transformed and data was filtered for two valid values in at least one group (each group contains triplicates). To solve the problem of missing values, data imputation was performed over the total matrix. For statistical evaluation, -log10(P values) were obtained by a two-sided two sample homoscedastic Student's t-test (Excel: ' =T.TEST(range1,range2,2,2))'.

Supplementary information

Table S4.1 | Significantly enriched proteins ($p < 0.05$, > 2-fold enrichment) in MRSA USA300 by probe **4** in comparison to DMSO-treated samples. Denoted by green dots in Figures 4.6 and S4.2.

Protein IDs	Protein names	Protein description	Gene names	**4** / DMSO	p-value
Q2FDS6	FphE	Uncharacterized hydrolase	SAUSA300_2518	108.24	0.000159
Q2FI93	FabH	3-oxoacyl-[acyl-carrier-protein] synthase 3	*fabH*	104.51	0.000109
A0A0H2XJL0	FphH	Carboxylesterase	*est*	67.42	0.002892
A0A0H2XHZ1	HZ1	Putative lysophospholipase	SAUSA300_0070	31.72	0.000860
A0A0H2XHD0	FphC	Hydrolase, alpha/beta hydrolase fold family	SAUSA300_1194	31.70	0.000178
A0A0H2XHH9	HH9	Putative lipase/esterase	SAUSA300_0641	30.60	0.000158
A0A0H2XJG5	FphB	Uncharacterized protein	SAUSA300_2473	20.71	0.000359
A0A0H2XFI2	FI2	Uncharacterized protein	SAUSA300_0321	16.51	0.001140
A0A0H2XIB7	IB7	Acetyl-CoA c-acetyltransferase	*vraB*	13.18	0.001232
A0A0H2XGQ4	A0A0H2XGQ4	Hydrolase, CocE/NonD family	SAUSA300_2531	6.67	0.000091
Q2FK94	ALDA	Putative aldehyde dehydrogenase AldA	*aldA*	5.99	0.000364
A0A0H2XHF0	FphA	Carboxylic ester hydrolase	*pnbA*	4.68	0.001104
A0A0H2XHE0	A0A0H2XHE0	Uncharacterized protein	SAUSA300_2093	4.06	0.000489
A0A0H2XFJ9	A0A0H2XFJ9	Peptidase, M20/M25/M40 family	SAUSA300_1460	3.21	0.001625
A0A0H2XJF4	A0A0H2XJF4	3-oxoacyl-[acyl-carrier-protein] synthase 2	*fabF*	2.99	0.001652
Q2FF06	ALDH	Putative aldehyde dehydrogenase	SAUSA300_2076	2.93	0.001234
A0A0H2XI47	FphI	Uncharacterized protein	SAUSA300_0430	2.73	0.000745
A0A0H2XFW4	A0A0H2XFW4	Peptidase, U32 family	SAUSA300_1569	2.73	0.002275
A0A0H2XFN6	FphF	Tributyrin esterase	*estA*	2.51	0.012576
Q2FK11	SCDA	Iron-sulfur cluster repair protein ScdA	*scdA*	2.23	0.000328
A0A0H2XG10	AdhE	Aldehyde-alcohol dehydrogenase	*adhE*	2.08	0.000095

Table S4.2 | Loadings protein inhibition PC2.

Protein inhibition	PC2 contribution (%)	direction
AdhE	**34**	**+**
FphC	**23**	**+**
IB7	16	-
FphB	11	+
FphH	6	-
F12	5	-
HZ1	5	-
HH9	0	-
FabH	0	-
FphE	0	-

Table S4.3 | Transposon mutant strain used, and their antibacterial susceptibility against compounds **1**-**3**, **5**-**7**

			MIC (μM)						
NTML strain	Locus	Transposon	**1**	**2**	**3**	**5**	**6**	**7**	Oxa2
		WT	6.25	12.5	0.8	>50	>50	>50	0.4
NE114	151	AdhE	6.25	12.5	0.8	>50	**25**	**12.5**	0.4
NE204	1194	FphC	6.25	12.5	0.8	>50	50	**25**	0.4
NE532	2473	FphB	6.25	12.5	0.8	>50	>50	>50	0.4
NE104	641	HH9	6.25	12.5	0.8 / 1.6	>50	50	50	0.4
NE1534	70	HZ1	6.25	12.5	0.8	>50	>50	>50	0.8
NE1227	560	IB7	6.25	25	0.4 / 0.8	>50	50	>50	0.8
NE1122	763	FphH	6.25	25	0.8	>50	>50	>50	0.8
NE1187	321	FI2	6.25	25	0.8	>50	>50	>50	0.4
NE1779	2518	FphE	6.25	6.25	0.8	>50	50	**12.5**	0.4

Table S4.4 | Minimum inhibitory concentrations of selected compounds against the **3**-resistant MRSA strains A/B obtained by serial passaging for 28 days from a MRSA USA300 background.

	MIC (μM)		
Compound	USA300	**3**-resistant A	**3**-resistant B
3	0.8	>50	>50
4	3.1	>50	>50
Meropenem	2.3	2.3	2.3
Vancomycin	0.7	0.7	0.7
Daptomycin	1.2	1.2	1.2
Rifampicin	0.015	0.015	0.015
Novobiocin	0.13	0.13	0.13
Chloramphenicol	12.5	12.5	12.5
Ciprofloxacin	>100	>100	>100
Oxa2	0.4	12.5	12.5

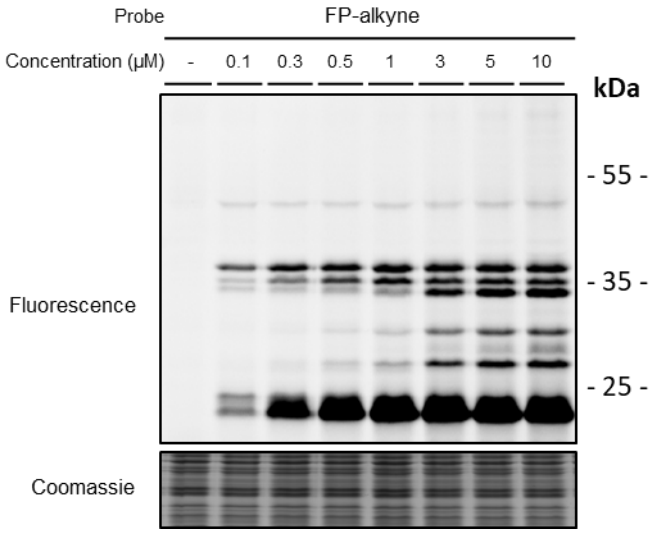

Figure S4.1 | *In situ* gel-based ABPP of a concentration range (0.1 – 10 μM) of the FP-alkyne probe in MRSA USA300.

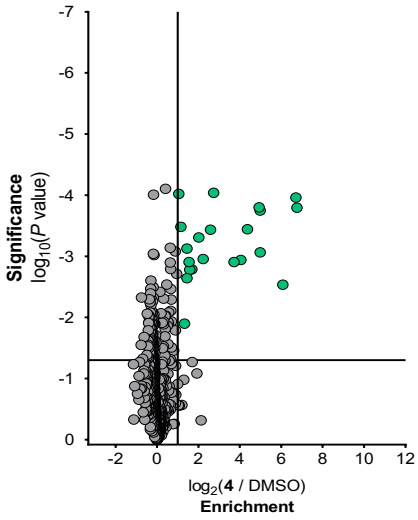

Figure S4.2 | Mass spectrometry data enrichment plot comparing labelled proteome of 3 µM **4**-treated MRSA to DMSO-treated MRSA. Green dots indicate proteins which are probe targets (> 2-fold enriched, $p < 0.05$). Probe targets annotated in Table S4.1.

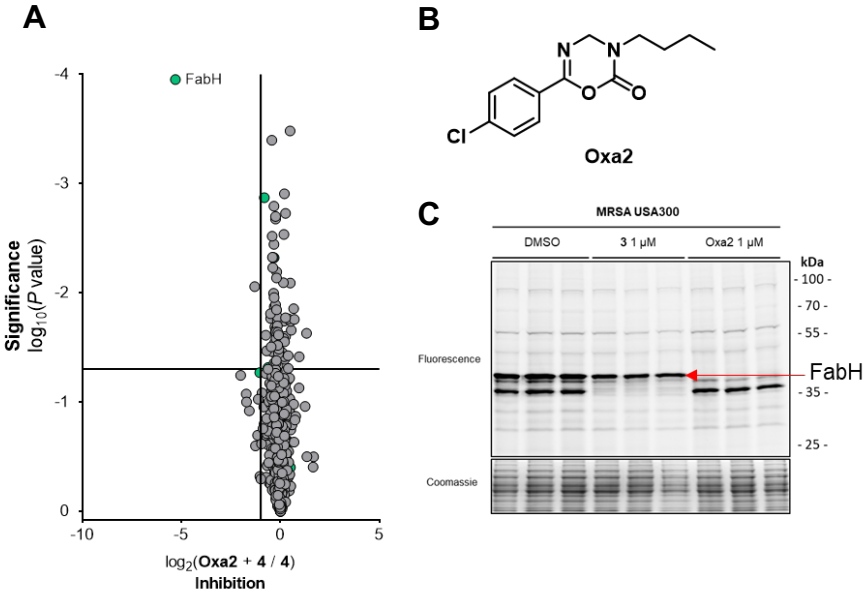

Figure S4.3 | Chemical proteomics data Oxa2 reveals FabH band on SDS-PAGE. **A)** Mass spectrometry data inhibition plot comparing labelled proteome of samples preincubated with Oxa2 (1 µM) followed by probe-labelling (3 µM) to solely probe-labelled samples. **B)** Chemical structure Oxa2. **C)** Gel-based competitive ABPP of indicated inhibitors followed by incubation with 3 µM probe **4**.

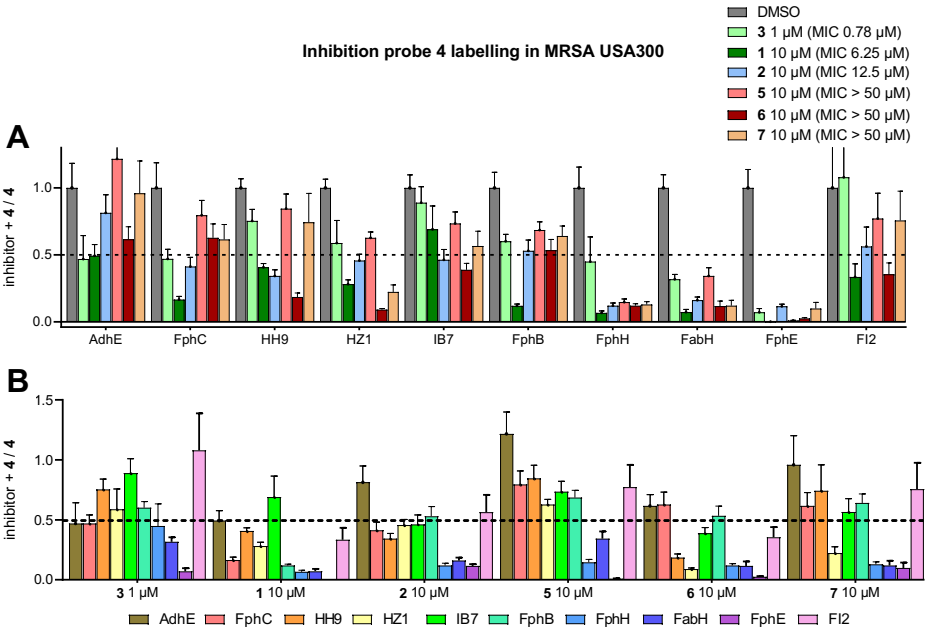

Figure S4.4 | Details inactive proteomics experiment. **A)** Bar graph inhibition profile per protein. **B)** Bar graph inhibition profile per inhibitor.

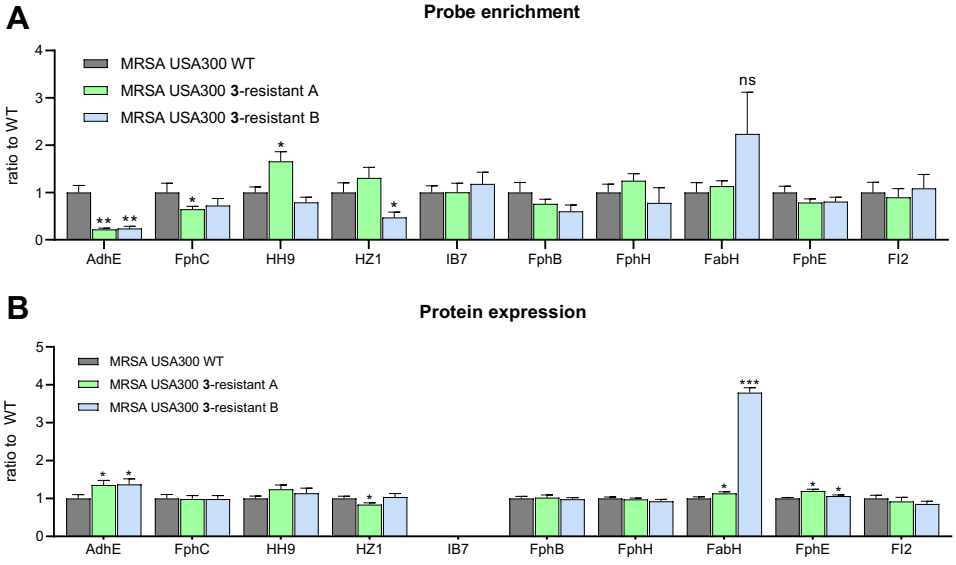

Figure S4.5 | Full bar chart proteomics data on **3**-resistant MRSA USA300 strains. **A)** Full graph probe **4** enrichment of targets. **B)** Full graph global protein expression. IB7 was not identified in any sample.

References

(1) Wright, M. H.; Sieber, S. A. Chemical Proteomics Approaches for Identifying the Cellular Targets of Natural Products. *Nat. Prod. Rep.* 2016, *33*, 681–708.

(2) May, K. L.; Grabowicz, M. The Bacterial Outer Membrane Is an Evolving Antibiotic Barrier. *Proc. Natl. Acad. Sci. U. S. A.* 2018, *115*, 8852–8854.

(3) Masi, M.; Réfregiers, M.; Pos, K. M.; Pagès, J. M. Mechanisms of Envelope Permeability and Antibiotic Influx and Efflux in Gram-Negative Bacteria. *Nat. Microbiol.* 2017, *2*.

(4) Amaral, L.; Martins, A.; Spengler, G.; Molnar, J. Efflux Pumps of Gram-Negative Bacteria: What They Do, How They Do It, with What and How to Deal with Them. *Front. Pharmacol.* 2014, *4 JAN*, 1–11.

(5) Moffat, J. G.; Vincent, F.; Lee, J. A.; Eder, J.; Prunotto, M. Opportunities and Challenges in Phenotypic Drug Discovery: An Industry Perspective. *Nat. Rev. Drug Discov.* 2017, *16*, 531–543.

(6) Van Esbroeck, A. C. M.; Janssen, A. P. A.; Cognetta, A. B.; Ogasawara, D.; Shpak, G.; Van Der Kroeg, M.; Kantae, V.; Baggelaar, M. P.; De Vrij, F. M. S.; Deng, H.; Allarà, M.; Fezza, F.; Lin, Z.; Van Der Wel, T.; Soethoudt, M.; Mock, E. D.; Den Dulk, H.; Baak, I. L.; Florea, B. I.; Hendriks, G.; De Petrocellis, L.; Overkleeft, H. S.; Hankemeier, T.; De Zeeuw, C. I.; Di Marzo, V.; Maccarrone, M.; Cravatt, B. F.; Kushner, S. A.; Van Der Stelt, M. Activity-Based Protein Profiling Reveals off-Target Proteins of the FAAH Inhibitor BIA 10-2474. *Science.* 2017, *356*, 1084–1087.

(7) Klaeger, S.; Heinzlmeir, S.; Wilhelm, M.; Polzer, H.; Vick, B.; Koenig, P. A.; Reinecke, M.; Ruprecht, B.; Petzoldt, S.; Meng, C.; Zecha, J.; Reiter, K.; Qiao, H.; Helm, D.; Koch, H.; Schoof, M.; Canevari, G.; Casale, E.; Re Depaolini, S.; Feuchtinger, A.; Wu, Z.; Schmidt, T.; Rueckert, L.; Becker, W.; Huenges, J.; Garz, A. K.; Gohlke, B. O.; Zolg, D. P.; Kayser, G.; Vooder, T.; Preissner, R.; Hahne, H.; Tõnisson, N.; Kramer, K.; Götze, K.; Bassermann, F.; Schlegl, J.; Ehrlich, H. C.; Aiche, S.; Walch, A.; Greif, P. A.; Schneider, S.; Felder, E. R.; Ruland, J.; Médard, G.; Jeremias, I.; Spiekermann, K.; Kuster, B. The Target Landscape of Clinical Kinase Drugs. *Science.* 2017, *358*, eaan4368-18.

(8) Bar-Peled, L.; Kemper, E. K.; Suciu, R. M.; Vinogradova, E. V.; Backus, K. M.; Horning, B. D.; Paul, T. A.; Ichu, T. A.; Svensson, R. U.; Olucha, J.; Chang, M. W.; Kok, B. P.; Zhu, Z.; Ihle, N. T.; Dix, M. M.; Jiang, P.; Hayward, M. M.; Saez, E.; Shaw, R. J.; Cravatt, B. F. Chemical Proteomics Identifies Druggable Vulnerabilities in a Genetically Defined Cancer. *Cell* 2017, *171*, 696-709.e23.

(9) Le, P.; Kunold, E.; Macsics, R.; Rox, K.; Jennings, M. C.; Ugur, I.; Reinecke, M.; Chaves-Moreno, D.; Hackl, M. W.; Fetzer, C.; Mandl, F. A. M.; Lehmann, J.; Korotkov, V. S.; Hacker, S. M.; Kuster, B.; Antes, I.; Pieper, D. H.; Rohde, M.; Wuest, W. M.; Medina, E.; Sieber, S. A. Repurposing Human Kinase Inhibitors to Create an Antibiotic Active against Drug-Resistant Staphylococcus Aureus, Persisters and Biofilms. *Nat. Chem.* 2020, *12*, 145–158.

(10) Hübner, I.; Shapiro, J. A.; Hoßmann, J.; Drechsel, J.; Hacker, S. M.; Rather, P. N.; Pieper, D. H.; Wuest, W. M.; Sieber, S. A. Broad Spectrum Antibiotic Xanthocillin X Effectively Kills Acinetobacter Baumannii via Dysregulation of Heme Biosynthesis. *ACS Cent. Sci.* 2021, acscentsci.0c01621.

(11) Murray, C. J.; Ikuta, K. S.; Sharara, F.; Swetschinski, L.; Robles Aguilar, G.; Gray, A.; Han, C.; Bisignano, C.; Rao, P.; Wool, E.; Johnson, S. C.; Browne, A. J.; Chipeta, M. G.; Fell, F.; Hackett, S.; Haines-Woodhouse, G.; Kashef Hamadani, B. H.; Kumaran, E. A. P.; McManigal, B.; Agarwal, R.; Akech, S.; Albertson, S.; Amuasi, J.; Andrews, J.; Aravkin, A.; Ashley, E.; Bailey, F.; Baker, S.; Basnyat, B.; Bekker, A.; Bender, R.; Bethou, A.; Bielicki, J.; Boonkasidecha, S.; Bukosia, J.; Carvalheiro, C.; Castañeda-Orjuela, C.; Chansamouth, V.; Chaurasia, S.; Chiurchiù, S.; Chowdhury, F.; Cook, A. J.; Cooper, B.; Cressey, T. R.; Criollo-Mora, E.; Cunningham, M.; Darboe, S.; Day, N. P. J.; De Luca, M.; Dokova, K.; Dramowski, A.; Dunachie, S. J.; Eckmanns, T.; Eibach, D.; Emami, A.; Feasey, N.; Fisher-Pearson, N.; Forrest, K.; Garrett, D.; Gastmeier, P.; Giref, A. Z.; Greer, R. C.; Gupta, V.; Haller, S.; Haselbeck, A.; Hay, S. I.; Holm, M.; Hopkins, S.; Iregbu, K. C.; Jacobs, J.; Jarovsky, D.; Javanmardi, F.; Khorana, M.; Kissoon, N.; Kobeissi, E.; Kostyanev, T.; Krapp, F.; Krumkamp, R.; Kumar, A.; Kyu, H. H.; Lim, C.; Limmathurotsakul, D.; Loftus, M. J.; Lunn, M.; Ma, J.; Mturi, N.; Munera-Huertas, T.; Musicha, P.; Mussi-Pinhata, M. M.; Nakamura, T.; Nanavati, R.; Nangia, S.; Newton, P.; Ngoun, C.; Novotney, A.; Nwakanma, D.; Obiero, C. W.; Olivas-Martinez, A.; Olliaro, P.; Ooko, E.; Ortiz-Brizuela, E.; Peleg, A. Y.; Perrone, C.; Plakkal, N.; Ponce-de-Leon, A.; Raad, M.; Ramdin, T.; Riddell, A.; Roberts, T.; Robotham, J. V.; Roca, A.; Rudd, K. E.; Russell, N.; Schnall, J.; Scott, J. A. G.; Shivamallappa, M.; Sifuentes-Osornio, J.; Steenkeste, N.; Stewardson, A. J.; Stoeva, T.; Tasak, N.; Thaiprakong, A.; Thwaites, G.; Turner, C.; Turner, P.; van Doorn, H. R.; Velaphi, S.; Vongpradith, A.; Vu, H.; Walsh, T.; Waner, S.; Wangrangsimakul, T.; Wozniak, T.; Zheng, P.; Sartorius, B.; Lopez, A. D.; Stergachis, A.; Moore, C.; Dolecek, C.; Naghavi, M. Global Burden of Bacterial Antimicrobial Resistance in 2019: A Systematic Analysis. *Lancet* 2022, *399*, 629–655.

(12) Tacconelli, E.; Carrara, E.; Savoldi, A.; Harbarth, S.; Mendelson, M.; Monnet, D. L.; Pulcini, C.; Kahlmeter, G.; Kluytmans, J.; Carmeli, Y.; Ouellette, M.; Outterson, K.; Patel, J.; Cavaleri, M.; Cox, E. M.; Houchens, C. R.; Grayson, M. L.; Hansen, P.; Singh, N.; Theuretzbacher, U.; Magrini, N.; Aboderin, A. O.; Al-Abri, S. S.; Awang Jalil, N.; Benzonana, N.; Bhattacharya, S.; Brink, A. J.; Burkert, F. R.; Cars, O.; Cornaglia, G.; Dyar, O. J.; Friedrich, A. W.; Gales, A. C.; Gandra, S.; Giske, C. G.; Goff, D. A.; Goossens, H.; Gottlieb, T.; Guzman Blanco, M.; Hryniewicz, W.; Kattula, D.; Jinks, T.; Kanj, S. S.; Kerr, L.; Kieny, M. P.; Kim, Y. S.; Kozlov, R. S.; Labarca, J.; Laxminarayan, R.; Leder, K.; Leibovici, L.; Levy-Hara, G.; Littman, J.; Malhotra-Kumar, S.; Manchanda, V.; Moja, L.; Ndoye, B.; Pan, A.; Paterson, D. L.; Paul, M.; Qiu, H.; Ramon-Pardo, P.; Rodríguez-Baño, J.; Sanguinetti, M.; Sengupta, S.; Sharland, M.; Si-Mehand, M.; Silver, L. L.; Song, W.; Steinbakk, M.; Thomsen, J.; Thwaites, G. E.; van der Meer, J. W.; Van Kinh, N.; Vega, S.; Villegas, M. V.; Wechsler-Fördös, A.; Wertheim, H. F. L.; Wesangula, E.; Woodford, N.; Yilmaz, F. O.; Zorzet, A. Discovery, Research, and Development of New Antibiotics: The WHO Priority List of Antibiotic-Resistant Bacteria and Tuberculosis. *Lancet Infect. Dis.* 2018, *18*, 318–327.

(13) Ben Ali, Y.; Chahinian, H.; Petry, S.; Muller, G.; Lebrun, R.; Verger, R.; Carrière, F.; Mandrich, L.; Rossi, M.; Manco, G.; Sarda, L.; Abousalham, A. Use of an Inhibitor to Identify Members of the Hormone-Sensitive Lipase Family. *Biochemistry* 2006, *45*, 14183–14191.

(14) Granchi, C.; Rizzolio, F.; Bordoni, V.; Caligiuri, I.; Manera, C.; Macchia, M.; Minutolo, F.; Martinelli, A.; Giordano, A.; Tuccinardi, T. 4-Aryliden-2-Methyloxazol-5(4H)-One as a New Scaffold for Selective Reversible MAGL Inhibitors. *J.*

Enzyme Inhib. Med. Chem. 2016, *31*, 137–146.

(15) Nguyen, P. C.; Delorme, V.; Bénarouche, A.; Guy, A.; Landry, V.; Audebert, S.; Pophillat, M.; Camoin, L.; Crauste, C.; Galano, J. M.; Durand, T.; Brodin, P.; Canaan, S.; Cavalier, J. F. Oxadiazolone Derivatives, New Promising Multi-Target Inhibitors against M. Tuberculosis. *Bioorg. Chem.* 2018, *81*, 414–424.

(16) Liu, Y.; Patricelli, M. P.; Cravatt, B. F. Activity-Based Protein Profiling: The Serine Hydrolases. *Proc. Natl. Acad. Sci. U. S. A.* 1999, *96*, 14694–14699.

(17) Janssen, A. P. A.; Van Der Vliet, D.; Bakker, A. T.; Jiang, M.; Grimm, S. H.; Campiani, G.; Butini, S.; Van Der Stelt, M. Development of a Multiplexed Activity-Based Protein Profiling Assay to Evaluate Activity of Endocannabinoid Hydrolase Inhibitors. *ACS Chemical Biology*. 2018.

(18) Van Rooden, E. J.; Florea, B. I.; Deng, H.; Baggelaar, M. P.; Van Esbroeck, A. C. M.; Zhou, J.; Overkleeft, H. S.; Van Der Stelt, M. Mapping in Vivo Target Interaction Profiles of Covalent Inhibitors Using Chemical Proteomics with Label-Free Quantification. *Nat. Protoc.* 2018, *13*, 752–767.

(19) Tyanova, S.; Temu, T.; Cox, J. The MaxQuant Computational Platform for Mass Spectrometry-Based Shotgun Proteomics. *Nat. Protoc.* 2016, *11*, 2301–2319.

(20) Lentz, C. S.; Sheldon, J. R.; Crawford, L. A.; Cooper, R.; Garland, M.; Amieva, M. R.; Weerapana, E.; Skaar, E. P.; Bogyo, M. Identification of a S. Aureus Virulence Factor by Activity-Based Protein Profiling (ABPP) Article. *Nat. Chem. Biol.* 2018, *14*, 609–617.

(21) Chen, L.; Keller, L. J.; Cordasco, E.; Bogyo, M.; Lentz, C. S. Fluorescent Triazole Urea Activity-Based Probes for the Single-Cell Phenotypic Characterization of Staphylococcus Aureus. *Angew. Chemie - Int. Ed.* 2019, *58*, 5643–5647.

(22) Wang, J.; Ye, X.; Yang, X.; Cai, Y.; Wang, S.; Tang, J.; Sachdeva, M.; Qian, Y.; Hu, W.; Leeds, J. A.; Yuan, Y. Discovery of Novel Antibiotics as Covalent Inhibitors of Fatty Acid Synthesis. *ACS Chem. Biol.* 2020, *15*, 1826–1834.

(23) Lai, C. Y.; Cronan, J. E. β-Ketoacyl-Acyl Carrier Protein Synthase III (FabH) Is Essential for Bacterial Fatty Acid Synthesis. *J. Biol. Chem.* 2003, *278*, 51494–51503.

(24) Wang, J.; Kodali, S.; Sang, H. L.; Galgoci, A.; Painter, R.; Dorso, K.; Racine, F.; Motyl, M.; Hernandez, L.; Tinney, E.; Colletti, S. L.; Herath, K.; Cummings, R.; Salazar, O.; González, I.; Basilio, A.; Vicente, F.; Genilloud, O.; Pelaez, F.; Jayasuriya, H.; Young, K.; Cully, D. F.; Singh, S. B. Discovery of Platencin, a Dual FabF and FabH Inhibitor with in Vivo Antibiotic Properties. *Proc. Natl. Acad. Sci. U. S. A.* 2007, *104*, 7612–7616.

(25) Luo, Y.; Yang, Y. S.; Fu, J.; Zhu, H. L. Novel FabH Inhibitors: A Patent and Article Literature Review (2000 2012). *Expert Opin. Ther. Pat.* 2012, *22*, 1325–1336.

(26) Meriläinen, G.; Poikela, V.; Kursula, P.; Wierenga, R. K. The Thiolase Reaction Mechanism: The Importance of Asn316 and His348 for Stabilizing the Enolate Intermediate of the Claisen Condensation. *Biochemistry* 2009, *48*, 11011–11025.

(27) Fuchs, S.; Pané-Farré, J.; Kohler, C.; Hecker, M.; Engelmann, S. Anaerobic Gene Expression in Staphylococcus Aureus. *J. Bacteriol.* 2007, *189*, 4275–4289.

(28) Lo, J.; Zheng, T.; Hon, S.; Olson, D. G.; Lynd, L. R. The Bifunctional Alcohol and Aldehyde Dehydrogenase Gene, AdhE, Is Necessary for Ethanol Production in Clostridium Thermocellum and Thermoanaerobacterium Saccharolyticum. *J. Bacteriol.* 2015, *197*, 1386–1393.

(29) Beckham, K. S. H.; Connolly, J. P. R.; Ritchie, J. M.; Wang, D.; Gawthorne, J. A.; Tahoun, A.; Gally, D. L.; Burgess, K.; Burchmore, R. J.; Smith, B. O.; Beatson, S. A.; Byron, O.; Wolfe, A. J.; Douce, G. R.; Roe, A. J. The Metabolic Enzyme AdhE Controls the Virulence of Escherichia ColiO157: H7. *Mol. Microbiol.* 2014, *93*, 199–211.

(30) Roch, M.; Gagetti, P.; Davis, J.; Ceriana, P.; Errecalde, L.; Corso, A.; Rosato, A. E. Daptomycin Resistance in Clinical MRSA Strains Is Associated with a High Biological Fitness Cost. *Front. Microbiol.* 2017, *8*, 1–9.

(31) Igler, C.; Rolff, J.; Regoes, R. Multi-Step vs. Single-Step Resistance Evolution under Different Drugs, Pharmacokinetics, and Treatment Regimens. *Elife* 2021, *10*, 1–24.